Journal of Catalysis 259 (2008) 240–249

Contents lists available at ScienceDirect

Journal of Catalysis

www.elsevier.com/locate/jcat

Evidence for the facile formation of nitrogen-containing compounds from NO_x and propene species on tungstated zirconia-based catalysts: Are these compounds active or spectator species in the selective catalytic reduction of NO_x by C_3H_6?

Nadia El Kolli [a,b], Claude Potvin [a,b], Cyril Thomas [a,b,*]

[a] UPMC Univ. Paris 06, UMR 7609, Laboratoire de Réactivité de Surface, 4 Place Jussieu, Case 178, F-75005 Paris, France
[b] CNRS, UMR 7609, Laboratoire de Réactivité de Surface, F-75005 Paris, France

ARTICLE INFO

Article history:
Received 10 June 2008
Revised 26 August 2008
Accepted 27 August 2008
Available online 27 September 2008

Keywords:
Lean deNO$_x$
Selective catalytic reduction
C_3H_6
Pd catalysts
WO_x–ZrO_2
TPSR of ad-NO$_x$
R–NO$_x$

ABSTRACT

The propene selective catalytic reduction (C_3H_6-SCR) of NO_x is investigated on WO_x–ZrO_2 and Pd/WO_x–ZrO_2. Temperature-programmed surface reaction (TPSR) experiments provide evidence of the decomposition of organic nitrogen-containing species formed through the interaction of C_3H_6 and ad-NO_x, for which a C/N ratio of 3 is estimated. The TPSR of preadsorbed NO_x in C_3H_6–O_2–He also suggests the presence of two R–NO_x species, C_3H_5–O–NO (propenyl nitrite) and C_3H_5–NO_2 (nitropropene), decomposing in distinct temperature regions. The addition of Pd to WO_x-ZrO_2 promotes the decomposition of nitropropene, whereas that of propenyl nitrite is scarcely affected. It is also suggested that R–NO_x are not active intermediates in C_3H_6-SCR on Pd/WZ catalysts but are more likely spectators. The activity for C_3H_6-SCR is attributed to Pd^0 species, formed by in situ reduction of oxidized Pd species by C_3H_6, via the well-established decomposition mechanism. In light of the new findings about the formation–decomposition of R–NO_x, results reported previously on a Pd/$Ce_{0.68}Zr_{0.32}O_2$ catalyst [C. Thomas, O. Gorce, C. Fontaine, J.-M. Krafft, F. Villain, G. Djéga-Mariadassou, Appl. Catal. B Environ. 63 (2006) 201], for which metal–support interactions prevent PdO_x reduction and C_3H_6-SCR reaction mechanism is different from that on Pd^0 sites, are widened.

1. Introduction

Although tungstated-zirconias (WO_x–ZrO_2) showed interesting catalytic properties in the skeletal isomerization of butane or pentane more than twenty years ago [1], their use as catalyst, or catalyst support, has been limited till the late nineties. Due to the strong Brønsted acidity of these materials [1–12], they have been used mainly for the isomerization of short-chain alkanes [2,6,13–24]. The redox character of W has also been demonstrated in the presence of H_2 and/or hydrocarbons [10,25]. It has been suggested that this redox character is the source of "temporary" Brønsted acidity which compensates for the negative charge of the polyoxotungstate domains [3–5,11,26,27].

Apart from the isomerization reactions for which the bifunctional character of the noble metal-promoted WO_x–ZrO_2 catalysts is well-suited, very few studies have been reported on the use of WO_x–ZrO_2-supported materials in the selective reduction of NO_x by hydrocarbons (HC-SCR) [28–32]. To our knowledge, palladium-promoted WO_x–ZrO_2 catalysts have been studied mainly for CH_4-SCR [28–32]. In their pioneering work, Resasco and coworkers also studied the influence of the reductant on the HC-SCR performances of Pd/WO_x–ZrO_2 catalysts [29]. These authors showed that important differences due to the nature of the reducing agent exist. The addition of W promotes CH_4-SCR, whereas it inhibits C_3H_6-SCR. In addition, the selectivity toward N_2 decreases when using C_3H_6 instead of CH_4. For a Pd/WO_x–ZrO_2 catalyst with 13.2 wt% W, it must be emphasized, however, that NO conversion in C_3H_6-SCR (approaching 90% at 435 °C) is about twice that found in CH_4-SCR under their experimental conditions.

On the basis of FTIR measurements, Weingand et al. have reported recently on the formation of an organic deposit through the interaction of nitrates and propene on WO_x–ZrO_2 [33]. These authors claim that the formed nitrogen-containing molecules, also reported as R–NO_x species in the literature, decompose to isocyanates which then react with NO + O_2 to yield N_2. The involvement of the formed R–NO_x species as intermediates of the HC-SCR has been reported in many studies [34–36]. Overall, this conclusion was reached based on the FTIR signature of R–NO_x compounds formed with a wide variety of hydrocarbons such as CH_4 [37–39], C_2H_5OH [40,41], C_3H_6 [42–56], C_3H_8 [45,53,57,58], C_4H_{10} [57] or $C_{10}H_{22}$ [59] on zeolite- and oxide-supported catalysts. Although

* Corresponding author at: UPMC Univ. Paris 06, UMR 7609, Laboratoire de Réactivité de Surface, 4 Place Jussieu, Case 178, F-75005 Paris, France. Fax: +33 1 44 27 60 33.
E-mail address: cyril.thomas@upmc.fr (C. Thomas).

0021-9517/$ – see front matter
doi:10.1016/j.jcat.2008.08.009

FTIR is a powerful technique to investigate the nature of the compounds formed on the catalyst surface, this technique (i) does not always provide detailed and reliable information on the thermal stability of the formed organic nitrogen-containing species and (ii) is inappropriate to determine their carbon to nitrogen stoichiometry.

This work aims at providing further insights on the facile formation and the decomposition of R–NO_x compounds on WO_x–ZrO_2-supported catalysts. By means of a reactivity approach, their thermal stability is ascertained and their carbon to nitrogen stoichiometry is estimated. On the Pd/WO_x–ZrO_2 catalyst, the results indicate that the organic nitrogen-containing compounds are more likely spectators in the C_3H_6-SCR reaction rather than intermediates. The role of Pd in R–NO_x decomposition is discussed and a comparison is provided with results published previously on $Ce_{0.68}Zr_{0.32}O_2$-supported samples [60].

2. Experimental

2.1. Catalyst synthesis

The tungstated zirconia (WO_x–ZrO_2: WZ) support was synthesized by suspending 3 g of commercial zirconium oxyhydroxide ($ZrO_x(OH)_{4-2x}$, XZO880/01), provided by MEL Chemicals (Manchester, UK), in 30 ml of an aqueous solution of ammonium metatungstate (0.49 g of $(NH_4)_6[W_{12}O_{40}H_2]$, Fluka). The suspension was stirred vigorously for 1 h at RT before being heated up to 110 °C for 20 h under reflux. Water was then gently evaporated and the material was dried in air at 110 °C for 18 h before being calcined up to 650 °C, with a heating rate of 5 °C min^{-1}, for 3 h under flowing air (33 mL min^{-1} g_{cat}^{-1}).

Two batches of tungstated zirconia-supported Pd catalysts (0.2 wt% Pd), namely Pd/WZ1 and Pd/WZ2, were prepared according to a method similar to that described for WZ. For the supported Pd catalysts, $Pd(NO_3)_2{\cdot}3H_2O$ (Johnson Matthey) was introduced to the zirconium oxyhydroxide/ammonium metatungstate suspension.

2.2. Catalyst characterization

The metal contents were determined by chemical analyses (CNRS—Vernaison). The specific surface areas were determined by physisorption of N_2 at 77 K using a Quantasorb Jr. dynamic system equipped with a thermal conductivity detector (TCD). The specific surface areas were calculated using the BET method. X-ray diffraction (XRD) patterns of WZ, Pd/WZ1 and Pd/WZ2 were collected on a Siemens D500 diffractometer with a CuK_α monochromatized radiation in 2θ from 12 to 70° with a scanning rate of 0.013° s^{-1}. Identification of the crystalline phases was made with the help of the Joint Committee Powder Diffraction Standard (JCPDS) files.

2.3. Catalytic runs

Prior to catalytic runs, the samples (0.5 g) were calcined in situ in O_2(20%)/He at 500 °C or 600 °C (3 °C min^{-1}) for 2 h with a flow rate of 100 mL_{NTP} min^{-1} (gas hour space velocity (GHSV) of about 17,000 h^{-1}), unless otherwise specified.

The experiments were carried out in a U-type quartz reactor (15 mm i.d.). The samples were held on plugs of quartz wool, and the temperature was controlled by a Eurotherm 2408 temperature controller using a K type thermocouple. Reactant gases were fed from independent mass flow controllers (Brooks 5850TR). The total flow was 230 mL_{NTP} min^{-1} which corresponds to a GHSV of about 40,000 h^{-1}.

Typically, the composition of the C_3H_6–NO–O_2 reaction mixture was: 480 ppm C_3H_6, 400 ppm NO and 7% O_2 in He. The reactants, diluted in He, were used as received and were fed from independent gas cylinders (Air Liquide).

The reactor outflow was continuously monitored using a combination of four detectors. A chemiluminescence NO_x analyzer (Thermo Environmental Instruments 42C-HT) allowed the simultaneous detection of both NO and NO_2. An Ultramat 6 IR analyzer was used to monitor N_2O. CO and CO_2 were analyzed using an infrared detector (Maihak 710). A FID detector (Thermo Environmental Instruments 51C-LT) was used to determine the concentration of hydrocarbons (HC). The response time of the detectors, including time lags due to gas transport in the lines from the outlet of the reactor to the detectors, were 0.25, 0.42 and 0.67 min for CO–CO_2–N_2O, NO–NO_2 and HC, respectively. Given that the transient experiments were carried out at a heating rate of 3 °C min^{-1}, these response times resulted in negligible temperature offsets of 0.8, 1.3 and 2.0 °C, respectively. Although it can be seen that the various traces were recorded within almost 1 °C difference only, the traces shown in this work were corrected from these very small differences in response time. We also checked that, under our experimental conditions, C_3H_6, CO and CO_2 had a negligible response on the N_2O IR analyzer. The conversion of NO_x was calculated as follows:

$$\text{Conversion of } NO_x\ (\%) = \frac{[NO_x]_{\text{inlet}} - [NO_x]_{\text{outlet}}}{[NO_x]_{\text{inlet}}},$$

where $[NO_x]_{\text{inlet}}$ and $[NO_x]_{\text{outlet}}$ are the concentrations of NO_x at the inlet and at the outlet of the reactor, respectively.

After exposure to the appropriate gas mixture at RT, temperature transient experiments were carried out from RT to 600 °C at a heating rate of 3 °C min^{-1}. Before the transient experiments, the catalyst samples were flushed in He at RT to remove weakly chemisorbed species. Various transient experiments were performed including (i) temperature-programmed surface reactions (TPSR) in O_2–He or C_3H_6–O_2–He, and (ii) temperature-programmed oxidations (TPO) in C_3H_6–O_2–He.

3. Results

3.1. Structural characterization of the catalysts

The composition of the catalysts and their specific surface areas are listed in Table 1. The amount of W in the synthesized materials is close to 13 wt%. The specific surface areas of the Pd/WZ samples is about 85 m^2 g^{-1}, whereas that of WZ is slightly lower (68 m^2 g^{-1}). This translates to tungsten surface densities of 6.8 and 4.8 W atoms nm^{-2} for the WZ and Pd/WZ samples, respectively.

The tetragonal ZrO_2 (t-ZrO_2) crystalline phase predominates for all samples, as indicated by the presence of diffraction peaks at 30.2, 35.3, 50.4, 60.3 and 62.9° (JCPDS file 50-1089) as shown in Fig. 1. This observation agrees with previous reports stating that the transformation of the t-ZrO_2 phase to the thermodynamically more stable monoclinic ZrO_2 phase (m-ZrO_2) can be delayed by the addition of transition metals [61,62]. The reflections of weak intensity observed at 28.3 and 31.5° are attributed to the presence of small amounts of m-ZrO_2 (JCPDS file 37-1484), the latter reflection being seen as a shoulder of the intense diffraction peak of the (111) plane of t-ZrO_2 at 30.2°. Detailed analysis of the 23–25° region clearly shows the presence of crystalline WO_3 (JCPDS file 32-1395) on the Pd-free WZ sample, with diffraction peaks at 23.1, 23.7 and

Table 1
Chemical elemental analyses and specific surface areas of the synthesized catalysts calcined at 650 °C for 3 h

Catalyst	W (wt%)	Pd (wt%)	Specific surface area (m^2 g^{-1})	δ (W at. nm^{-2})
WZ	14.2	–	68	6.8
Pd/WZ1	12.8	0.20	89	4.7
Pd/WZ2	11.9	0.19	80	4.9

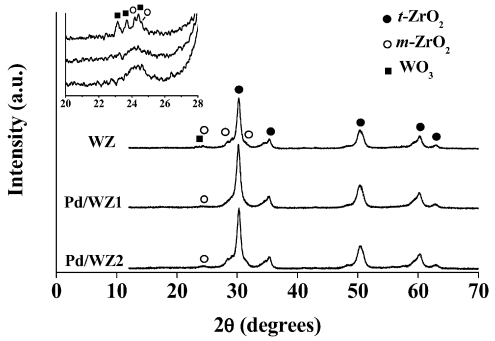

Fig. 1. XRD patterns of the catalysts after calcination at 650 °C for 3 h.

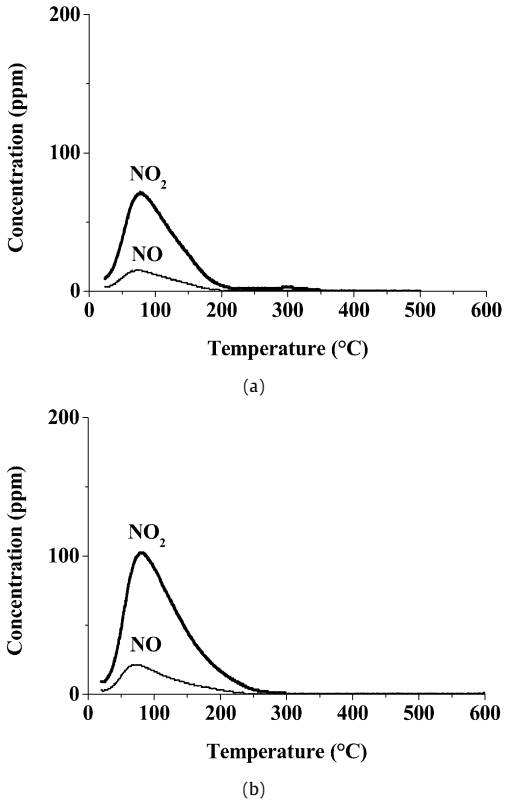

Fig. 2. NO_x temperature-programmed surface reaction profiles in O_2–He (7% in He) after exposure of the sample to NO–O_2–He (400 ppm—7%—balance) at RT: (a) for 40 min on WZ, (b) for 90 min on Pd/WZ1.

24.4° (insert of Fig. 1). In contrast, the Pd/WZ catalysts only show a broad reflection centered at 24.2°, which is likely the diffraction of the (110) and (011) planes of m-ZrO_2. These results suggest that the tungsten phase is well dispersed on the Pd/WZ samples and that the introduction of Pd seems to have a promoting effect on the tungsten dispersion. This conclusion is supported by the fact that the WO_3 reflections were also observed (not shown) in the case of a second batch of WZ exhibiting a specific surface area (85 $m^2\,g^{-1}$) comparable to those reported for the Pd/WZ catalysts (Table 1). The fact that Pd/WZ2 shows a slightly greater content of m-ZrO_2 compared to Pd/WZ1 may result from slight differences in the calcination conditions.

3.2. Catalytic reactivity

3.2.1. Adsorption of NO–O_2 — TPSR in O_2–He

Fig. 2 shows the NO_x profiles in O_2–He (7% in He) obtained on WZ (Exp. 1) and Pd/WZ1 (Exp. 4) after contact with NO–O_2–He (400 ppm—7%—balance). It should be noted that the profiles observed on Pd/WZ2 (Exp. 10, not shown) are similar to those reported in Fig. 2. On Pd/WZ1, it was observed that the TPD in He (not shown) does not differ from the TPSR in O_2–He (Fig. 2b).

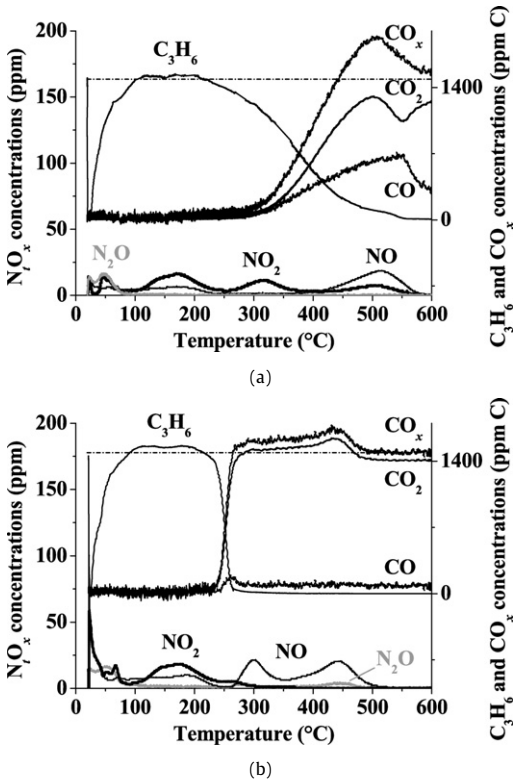

Fig. 3. Temperature-programmed surface reaction in C_3H_6–O_2–He (480 ppm—7%—balance) after exposure to NO–O_2–He (400 ppm—7%—balance) at RT: (a) for 40 min on WZ, (b) for 95 min on Pd/WZ1.

For all samples, NO and NO_2 releases occur at about 70 and 80 °C, respectively. The amounts of NO_2 produced in the TPSR in O_2–He are much greater than those of NO (Table 2, Exps. 1, 4 and 10) and account for 80% of the total amount of NO_x produced. The reason for which the amount of NO_x released in the TPSR in O_2–He is slightly greater for Pd/WZ1 (Exp. 4: 0.96 μmol m^{-2}) than for WZ and Pd/WZ2 (Exps. 1 and 10: 0.80 μmol m^{-2}) remains unclear.

3.2.2. Interaction between C_3H_6 and the formed ad-NO_xspecies

3.2.2.1. Adsorption of NO–O_2 — TPSR in C_3H_6–O_2–He Fig. 3 shows the profiles obtained in C_3H_6–O_2–He (480 ppm—7%—balance) for WZ (Exp. 2) and Pd/WZ1 (Exp. 5) after exposure to NO–O_2–He (400 ppm—7%—balance). In these experiments, the temperature was ramped as soon as the samples previously saturated with ad-NO_x species were exposed to the C_3H_6–O_2–He mixture. C_3H_6 adsorbs up to about 100 °C and part of the chemisorbed propene species then desorb up to 215 °C, the temperature at which C_3H_6 oxidation begins. C_3H_6 oxidation is much steeper on Pd/WZ1 than on WZ. Complete conversion of C_3H_6 occurs at 550 °C on WZ, whereas propene oxidation is almost complete at 265 °C on Pd/WZ1 (Fig. 3b). CO_2 is the major product from C_3H_6 oxidation on Pd/WZ1, while significant CO production is observed from 330 to 600 °C on WZ (Fig. 3a). One may also note the presence of CO_x production at high temperatures on Pd/WZ1 (265–500 °C) and WZ (440–600 °C). On Pd/WZ1, the carbon mass balance was found to be 100% within 5% of confidence.

The profiles of the N_tO_x species (NO, NO_2 and N_2O) were more complicated. First, the sharp features observed concomitant to the exposure of Pd/WZ1 to C_3H_6–O–He at RT (Fig. 3b) has been attributed to an artifact, as this feature is not observed either on WZ

Table 2
Amounts of NO_x ($NO + NO_2$), N_2O or CO_x ($CO + CO_2$) released in the TPSR experiments after exposure of the catalysts to $NO–O_2$ (400 ppm–7% in He) or the TPO experiments

Catalysts	Experiments	Amounts of released species ($\mu mol\, m^{-2}$)						
		NO	NO_2	NO_x	N_2O	$NO_x + 2N_2O$	N (%)[a]	CO_x
WZ	1. TPSR in O_2–He	0.14	0.67	0.81	0.00	0.81	–	–
	2. TPSR in C_3H_6–O_2–He	0.31	0.37	0.68	0.07	0.82	100	3.91
	3. TPO in C_3H_6–O_2–He	–	–	–	–	–	–	10.71
Pd/WZ1	4. TPSR in O_2–He	0.17	0.79	0.96	0.00	0.96	–	–
	5. TPSR in C_3H_6–O_2–He	0.35	0.18	0.53	0.12	0.77	80	2.67
	6. TPSR in C_3H_6–O_2–He after flushing under C_3H_6–O_2–He at RT for 25 min	0.37	0.19	0.56	0.12	0.80	83	2.68
	7. TPO in C_3H_6–O_2–He	–	–	–	–	–	–	2.63
	8. TPSR in C_3H_6–O_2–He with the removal of C_3H_6 at 226 °C	0.31	0.21	0.52	0.10	0.72	75	1.93
	9. TPO in C_3H_6–O_2–He with the removal of C_3H_6 at 190 °C	–	–	–	–	–	–	1.32
Pd/WZ2	10. TPSR in O_2–He	0.17	0.63	0.80	0.00	0.80	–	–
	11. TPSR in C_3H_6–O_2–He	0.27	0.15	0.42	0.11	0.64	80	2.56
	12. TPSR in C_3H_6–O_2–He with the removal of C_3H_6 at 90 °C	0.30	0.15	0.45	0.09	0.63	79	1.33
	13. TPO in C_3H_6–O_2–He with the removal of C_3H_6 at 90 °C	–	–	–	–	–	–	0.74
	14. TPSR in O_2–He after exposure to C_3H_6–NO–O_2 at RT	0.19	0.10	0.29	0.10	0.49	–	1.00
	15. TPSR in O_2–He after exposure to C_3H_6–O_2 at RT	–	–	–	–	–	–	0.49

[a] N referred to as the amount of released N_tO_x species in the TPSR in C_3H_6–O_2–He relative to that released in the TPSR in O_2–He.

(Fig. 3a) or on Pd/WZ2 (Exp. 11, not shown). This is further supported by the lack of N_tO_x production at RT for the experiment in which the NO_x-saturated Pd/WZ1 sample was previously flushed by C_3H_6–O–He (Exp. 6, profiles not shown). On Pd/WZ1 (Fig. 3b), two broad NO features are observed from 50 to 250 and 270 to 500 °C. Two NO_2 peaks are seen at 50 and 170 °C and low concentrations of N_2O are monitored at low temperatures from RT to 80 °C, and at 280 and 450 °C. The NO_x profiles for WZ (Fig. 3a) differ markedly from those for Pd/WZ1 for temperatures greater than 250 °C. NO is only detected above 400 °C with a maximum at 500 °C, two NO_2 peaks are observed at 315 and 515 °C, while N_2O is not produced above 250 °C.

The TPSR in C_3H_6–O_2–He performed on a NO_x-saturated Pd/WZ1 sample previously contacted with C_3H_6–O_2–He at RT for 25 min (Exp. 6, profiles not shown) is similar to that shown in Fig. 3b. The results for Pd/WZ2 (Exp. 11, profiles not shown) agree qualitatively with those for Pd/WZ1 (Fig. 3b). On Pd/WZ2, the CO_2 profile is, however, slightly more intense at 255 °C and the N_tO_x profiles are shifted to slightly lower temperatures compared with those shown in Fig. 3b.

3.2.2.2. Adsorption of NO–O_2 — TPSR in C_3H_6–O_2–He with the removal of C_3H_6 in the course of the TPSR Fig. 4 shows the TPSR in C_3H_6–O_2–He, with the removal of C_3H_6 at various temperatures, performed on NO_x-saturated Pd/WZ samples. Fig. 4a shows analogous profiles as those observed in the case of the TPSR experiment described in Section 3.2.2.1 on Pd/WZ1 (Fig. 3b). Despite the fact that C_3H_6 was removed from the gas feed at 226 °C, CO_2 production is observed from 250 to 500 °C. In this temperature range, concomitant formation of NO is observed together with trace amounts of NO_2 up to 350 °C and N_2O at 300 and 460 °C. As shown in Fig. 4b, the removal of C_3H_6 at 90 °C does not affect the profiles significantly. As also mentioned earlier for the TPSR in C_3H_6–O_2–He without removal of C_3H_6 (Section 3.2.2.1), the experiment in which C_3H_6 was removed from the gas feed at 90 °C on Pd/WZ2 (Exp. 12, Fig. 4b) agrees with that described on Pd/WZ1, for which C_3H_6 was removed from the gas feed at 226 °C (Fig. 4a). On Pd/WZ2, the CO_2 profile is, however, slightly more intense at 280 °C and the N_tO_x profiles are shifted to slightly lower temperatures compared with those for Pd/WZ1 (Fig. 4a).

3.2.2.3. Coadsorption of C_3H_6–NO–O_2 — TPSR in O_2–He Exposure of Pd/WZ2 at RT to the complete C_3H_6–NO–O_2–He mixture followed by the TPSR in O_2–He (Exp. 14, Fig. 4c) resulted in the concomitant production of CO_2 and NO from 280 to 500 °C. Small amounts of C_3H_6 desorb from RT to 360 °C (insert of Fig. 4c).

3.2.2.4. Comparison of the TPSR in O_2–He with those in C_3H_6–O_2–He Table 2 summarizes the amounts of N_tO_x and CO_x species produced in the TPSR experiments on WZ (Exp. 2), Pd/WZ1 (Exps. 5, 6 and 8) and Pd/WZ2 (Exps. 11, 12 and 14).

On the Pd/WZ catalysts, the most striking difference between the TPSR experiments in O_2–He and those in C_3H_6–O_2–He is that NO is the major species in the latter experiments, whereas NO_2 is the major species in the former experiments. On WZ, the amount of NO_2 formed in the presence of C_3H_6 (Table 2, Exp. 2) decreases significantly compared to that in the absence of C_3H_6 (Table 2, Exp. 1). On the Pd/WZ catalysts, the total amounts of N_tO_x species produced in the TPSR involving C_3H_6 (Table 2, Exps. 5, 6, 8, 11, 12 and 14), taking into account that N_2O originates from the recombination of two NO_x molecules, are always lower than those produced in the TPSR carried out in the absence of C_3H_6 (Table 2, Exps. 4 and 10). In contrast, the total amount of N_tO_x species is not influenced by the presence of C_3H_6 on WZ (Table 2, Exps. 1 and 2). This indicates that part of the NO_x chemisorbed on the Pd/WZ catalysts is reduced to N_2 in the course of the TPSR in C_3H_6–O_2–He. The amount of NO_x converted to N_2 in the presence of C_3H_6 is estimated to be 20% of the amount of NO_x released in the absence of C_3H_6. It is also interesting to note that release of adsorbed NO_x species occurs at much higher temperatures in the TPSR in C_3H_6–O_2–He (Fig. 5). The comparison of Figs. 3a and 3b shows that the introduction of Pd has a dramatic influence on both the temperature at which N_tO_x species are produced and their distribution.

The amount of CO_x released in the TPSR in C_3H_6–O_2–He is the greatest on WZ (3.91 $\mu mol\, m^{-2}$, Table 2). On the Pd/WZ catalysts, Table 2 shows that this quantity decreases as the temperature at which C_3H_6 is removed from the gas feed decreases.

3.2.3. Temperature-programmed oxidation of C_3H_6 by O_2

Fig. 6 shows temperature-programmed oxidation of C_3H_6 by O_2 on WZ and Pd/WZ1. The TPO profiles resemble those described for the TPSR in C_3H_6–O_2–He (Section 3.2.2.1). C_3H_6 adsorbs up to about 90 °C after which part of the chemisorbed propene species desorb up to 160 °C, the temperature at which C_3H_6 starts to oxidize. Fig. 6 also shows that C_3H_6 oxidation is much steeper on Pd/WZ1 than on WZ, as observed in the TPSR in C_3H_6–O_2–He (Fig. 3). Complete conversion of C_3H_6 occurs at 500 and 225 °C on WZ and Pd/WZ1, respectively. CO_2 is the major product from C_3H_6 oxidation on Pd/WZ1, while significant CO production is observed from 270 to 600 °C on WZ (Fig. 6a). One may also observe a broad CO_x production at high temperatures on Pd/WZ1 (236–475 °C) or WZ (400–600 °C).

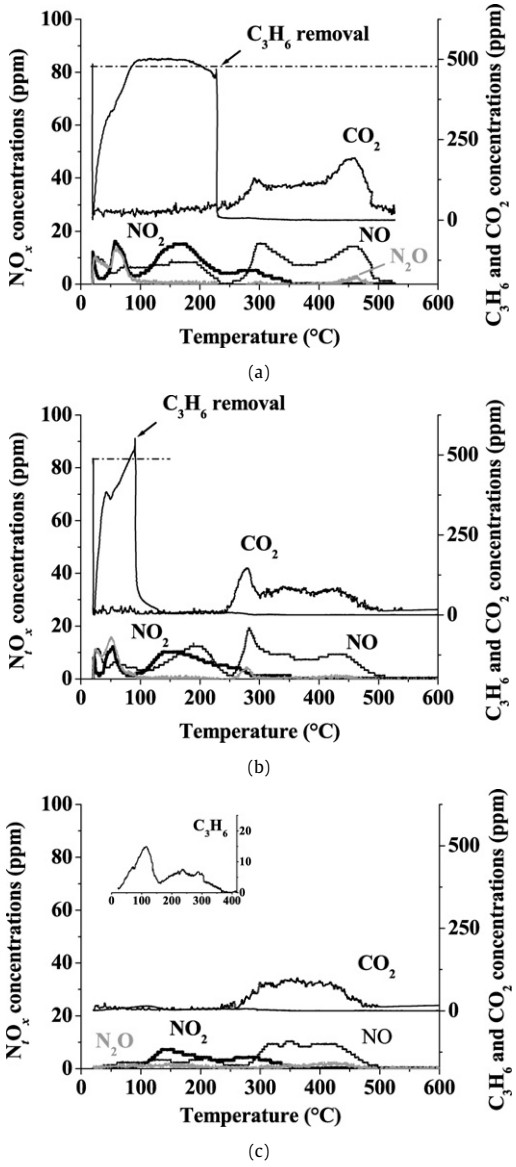

Fig. 4. Temperature-programmed surface reaction in C_3H_6–O_2–He (480 ppm—7%—balance), after exposure of the Pd/WZ catalysts to NO–O_2–He (400 ppm—7%—balance) at RT: (a) on Pd/WZ1 with the removal of C_3H_6 at 226 °C, (b) on Pd/WZ2 with the removal of C_3H_6 at 90 °C or (c) in O_2–He (7% in He) after exposure of Pd/WZ2 to C_3H_6–NO–O_2–He (480 ppm—400 ppm—7%—balance) at RT.

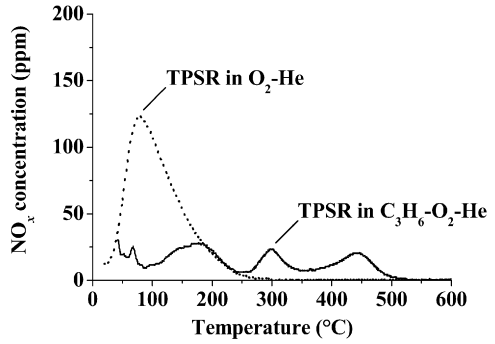

Fig. 5. Comparison of the NO_x profiles on Pd/WZ1: TPSR in O_2–He (7% in He), TPSR in C_3H_6–O_2–He (480 ppm—7%—balance).

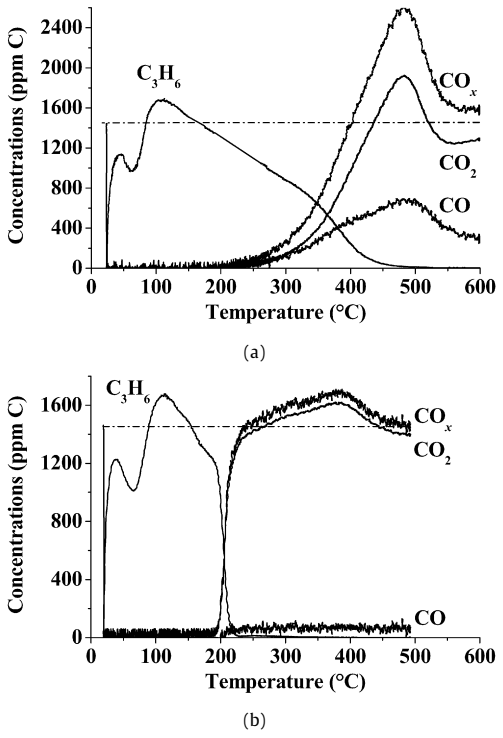

Fig. 6. Temperature-programmed oxidation of C_3H_6 (480 ppm C_3H_6—7% O_2—balance He) on (a) WZ, (b) Pd/WZ1.

TPO mainly differ from TPSR in C_3H_6–O_2–He (Fig. 3) by the presence of a pronounced C_3H_6 chemisorption at about 65 °C and shifting of the C_3H_6 conversion profiles by about 40–50 °C lower, as illustrated in Fig. 7 for Pd/WZ1. Concurrently, the CO_x profiles also shift to lower temperatures in the TPO experiments. A similar trend was observed for WZ and Pd/WZ2. Below 50 °C, the quantity of chemisorbed C_3H_6 is lower in the TPO than that in the TPSR in C_3H_6–O_2–He (Fig. 7). The TPO experiment in which C_3H_6 is removed at 190 °C (Fig. 8) agrees well with that shown in Fig. 6b. C_3H_6 adsorption and desorption features are observed from RT to 170 °C and CO_2 production occurs from 250 to 400 °C with a maximum at 385 °C.

The amounts of CO_x species released in the TPO experiments are listed in Table 2 (Exps. 3, 7, 9 and 13). WZ exhibits a peculiar behavior compared to the Pd/WZ samples, as the amount of released CO_x species is much greater in the TPO experiment (Table 2, Exp. 3) than in the TPSR in C_3H_6–O_2–He (Table 2, Exp. 2). In contrast, the amounts of CO_x species formed in the TPO experiments (Table 2, Exps. 7, 9 and 13) are lower than those produced in the TPSR in C_3H_6–O_2–He (Table 2, Exps. 5 or 6, 8 and 12). As also observed for the TPSR in C_3H_6–O_2–He, the amount of CO_x released in the TPO decreases as the temperature at which C_3H_6 is removed from the feed decreases.

3.2.4. Temperature-programmed oxidation of C_3H_6 by O_2 after adsorption of C_3H_6 at RT

Fig. 9 shows the TPO in O_2–He (7%, balance He) of C_3H_6 preadsorbed at RT on Pd/WZ2 (Exp. 15). As in the case of Exps. 9 (Fig. 8) and 13 (not shown), a broad CO_2 peak is observed from 250 to 400 °C. It is worthwhile to note that C_3H_6 desorption also occurs but in a much narrower temperature range, from RT to 150 °C, than that found in the TPSR in O_2–He after coadsorption of NO_x and C_3H_6 (Exp. 14, insert of Fig. 4c). In addition, the amount of desorbed C_3H_6 is greater on the Pd/WZ2 sample exposed to C_3H_6 in the absence of NO_x (Fig. 9) compared to that released from the same sample exposed to the complete C_3H_6–NO–O_2–He mixture (Fig. 4c).

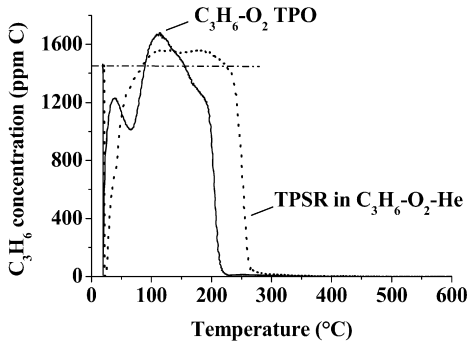

Fig. 7. Comparison of C_3H_6 oxidation (480 ppm C_3H_6—7% O_2—balance He) on Pd/WZ1: (a) calcined at 600 °C for 2 h, (b) calcined at 600 °C for 2 h and exposed to NO–O_2–He (400 ppm—7%—balance) at RT.

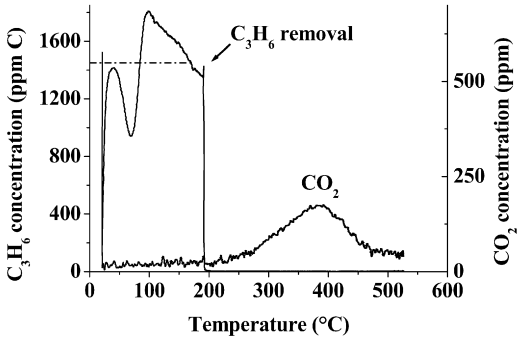

Fig. 8. Temperature-programmed oxidation of C_3H_6 (480 ppm C_3H_6—7% O_2—balance He) with the removal of C_3H_6 at 190 °C on Pd/WZ1.

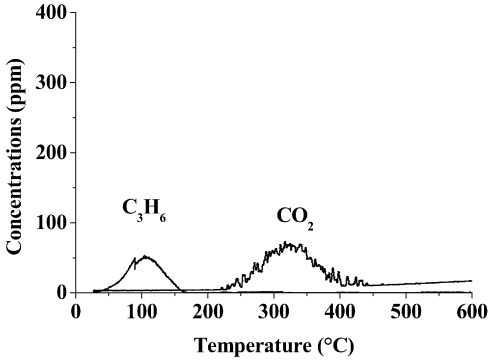

Fig. 9. Temperature-programmed oxidation (7% O_2 in He) of C_3H_6 preadsorbed at RT (480 ppm C_3H_6—7% O_2, balance He) on Pd/WZ2.

3.2.5. Steady-state NO–C_3H_6–O_2 reaction

It was determined that NO_x reduction does not occur over WZ, whereas C_3H_6 oxidation starts at 300 °C and is completed at 525 °C (results not shown). Fig. 10 shows the steady-state conversions of C_3H_6 and NO_x recorded in two separate runs on Pd/WZ1. In the first run (Fig. 10, solid symbols), the catalyst is heated at 250 °C under the C_3H_6–NO–O_2 mixture. The activity of the catalyst is measured at this temperature before the temperature is decreased to 190 °C. The conversions are then obtained by stepwise increase of the temperature to 210, 230, 250 and 300 °C. In the second run (Fig. 10, open symbols), the sample is heated up to 190 °C under the C_3H_6–NO–O_2 mixture and the activity of the catalyst is measured at this temperature before stepwise increase of the temperature to 210, 230 and 250 °C.

The introduction of Pd promotes the conversions of C_3H_6 and NO_x. NO_x conversion reaches a maximum of 17% at 250 °C and

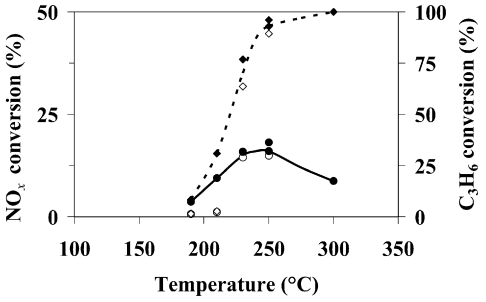

Fig. 10. Steady-state catalytic conversions of C_3H_6 (◆,◇) and NO_x (●,○) in the course of the C_3H_6–NO–O_2–He reaction (480 ppm—400 ppm—7%—balance) on Pd/WZ1: (solid symbols) run 1, (open symbols) run 2 after calcination of the sample at 600 °C for 2 h following run 1.

then decreases as C_3H_6 combustion becomes predominant. The N_2 selectivity, expressed as the $N_2/(N_2 + N_2O)$ ratio, is about 50%. C_3H_6 conversion starts at 190 °C and approaches 100% at 250 °C. Surprisingly, C_3H_6 and NO_x conversions recorded in run 2 are clearly different from those found in run 1 for reaction temperatures below 230 °C, whereas those at 230 °C and above agree well for both runs. This suggests that activation of Pd/WZ1 occurs under the C_3H_6–NO–O_2 mixture at temperatures above 210 and below 230 °C.

4. Discussion

4.1. Formation–decomposition of nitrogen-containing organic species

The fact that NO_x profiles are observed at much greater temperatures in the TPSR in C_3H_6–O_2–He (Figs. 3 and 4) than in the TPSR in O_2–He (Fig. 2), and that the amounts of released N_tO_x species does not differ much between both TPSR experiments (Table 2) testifies unambiguously (Fig. 5) of the decomposition of organic nitrogen-containing species formed through the interaction of C_3H_6 and ad-NO_x.

This conclusion is supported by the concomitant production of NO_x and of CO_x (Figs. 3 and 4), as was also noticed by Rebrov et al. in the reaction between NO_x and C_3H_8 on Cu/ZSM-5 [63] and Burch et al. in the NO_x-CH_3OH reaction on alumina-based catalysts [64]. From the TPO results (Figs. 6, 8 and 9), CO_x production is also observed in the absence of ad-NO_x species in a range of temperature comparable to that reported in the TPSR in C_3H_6–O_2–He. Rebrov et al. and Burch et al. did not detect CO_x in the temperature range where organic nitrogen-containing species decomposition occurs [63,64]. Concerning this, a comparison of the experiments in which Pd/WZ2 was exposed to C_3H_6–NO–O_2–He and C_3H_6–O_2–He at RT (Exps. 14 and 15) followed by TPSR in O_2–He (Figs. 4c and 9, respectively) and the comparison of the amounts of CO_x produced in the TPSR in C_3H_6–O_2–He with those of the TPO in O_2–He on the Pd/WZ catalysts (Table 2, Exps. 5–9 and 12–15) provide further information. First, the amounts of CO_x produced in the TPSR in C_3H_6–O_2–He are always greater than those found in the TPO in O_2–He (Table 2). Second, the comparison between Exps. 14 and 15 (Figs. 4c and 9) indicates that the NO_x species strongly inhibits C_3H_6 chemisorption, which agrees with previous conclusions drawn by Weingand et al. [33]. This suggests that the amounts of CO_x released in the TPO experiments must be slightly overestimated compared to those found in the TPSR in C_3H_6–O_2–He. These comparisons, thus, support that extra amounts of CO_x are produced by the decomposition of the organic nitrogen-containing species above 250 °C.

Table 3
Amounts of NO and CO_2 released in the 250–500 °C region in the experiments reported in Table 2

Catalysts	Experiments	Amounts of released species (μmol m^{-2})		ΔCO_2[a]	ΔCO_2/NO
		NO	CO_2		
Pd/WZ1	8. TPSR in C_3H_6–O_2–He with the removal of C_3H_6 at 226 °C	0.19	1.93		
	9. TPO in C_3H_6–O_2–He with the removal of C_3H_6 at 190 °C	–	1.32		
				0.61	3.2
Pd/WZ2	12. TPSR in C_3H_6–O_2–He with the removal of C_3H_6 at 90 °C	0.18	1.33		
	13. TPO in C_3H_6–O_2–He with the removal of C_3H_6 at 90 °C	–	0.74		
				0.58	3.2
	14. TPSR in O_2–He after exposure to C_3H_6–NO–O_2 at RT	0.14	1.00		
	15. TPSR in O_2–He after exposure to C_3H_6–O_2 at RT	–	0.49		
				0.51	3.6

[a] ΔCO_2 referred to as the difference between the amount of CO_2 released in the TPSR in C_3H_6–O_2–He and that released in the TPO in C_3H_6–O_2–He.

4.2. Estimation of the C/N ratio of the nitrogen-containing organic species

If the decomposition of alcohols–NO_x adducts has also been reported unambiguously previously [64,65] on the basis of sharp desorptions of NO_x, mainly NO, and CO_2, very few studies tackled the challenging issue consisting in the determination of the C/N ratio of the organic nitrogen-containing species formed via the interaction of NO_x and various hydrocarbons [59,63,66]. To the best of our knowledge, the present study is the first literature report in which the C/N ratio is estimated by transient experiments using propene as a reductant. It would be the second if one considers the elegant work of Rebrov et al. which involves propane as the reductant [63]. From the TPSR and the TPO experiments in C_3H_6–O_2–He, an estimation of the C/N ratio may be obtained.

Table 3 lists the amounts of NO and CO_x, mainly CO_2, released in the aforementioned experiments in the 250–500 °C temperature domain, within which the decomposition of the organic nitrogen-containing species occurs. It can be seen that the amounts of NO produced in the TPSR in C_3H_6–O_2–He remains fairly constant irrespective of the temperature at which C_3H_6 is removed from the feed (Exps. 8 and 12). The amount of NO released in the TPSR in C_3H_6–O_2–He after exposure of Pd/WZ2 to a C_3H_6–NO–O_2–He mixture at RT (Table 3, Exp. 14) is slightly lower than those found when Pd/WZ samples are exposed to NO–O_2–He (Exps. 8 and 12). This could either be that propene competes with the catalytic sites involved in the adsorption of NO_x or that the quantity of propene deposited at RT is below that required from a stoichiometric point of view to react with the amount of NO_x adsorbed under the present experimental conditions.

As indicated earlier, the amount of CO_2 released (i) decreases as the temperature at which propene is removed from the feed decreases and (ii) is always greater in the TPSR in C_3H_6–O_2–He compared to that found in the TPO in C_3H_6–O_2–He. These observations may be likely attributed to (i) lower coking of the catalyst samples with the decrease in the temperature at which propene is removed from the feed and (ii) the fact that adsorbed NO_x react with propene to form organic nitrogen-containing species which most probably prevent further coking of the catalyst since their decomposition occurs at elevated temperatures.

From the difference between the amounts of CO_2 released in the TPSR in C_3H_6–O_2–He with those released in the TPO in C_3H_6–O_2–He (Table 3, ΔCO_2), the C/N ratio was estimated to be about 3 for the formed organic nitrogen-containing species. This value agrees with those reported previously by Brosius et al. and Rebrov et al. using decane and propane as reductants [59,63], respectively. In contrast, this value differs markedly from that reported by Hayes et al. [66]. In the latter study, however, the much greater C/N ratio, i.e. 5.3, may be attributed to coking of the acidic catalyst by propene, which was not taken into account by the authors. The fact that the C/N ratios are slightly greater than 3 can be assigned to two antagonist phenomena: (i) The amounts of N-containing products must be slightly underestimated, as the HC-SCR reaction also occurs in the temperature domain of interest (Fig. 10) and as the amounts of N_2O and N_2, the latter could not be measured with a sampling rate compatible with the conditions of the transient experiments, are not included in the calculation of the C/N ratio, as was also the case in the work of Rebrov et al. [63]. (ii) As discussed above, the amounts of CO_2 released in the TPO in C_3H_6–O_2–He are slightly overestimated, leading to a slight underestimation of ΔCO_2. The latter would also account for the more pronounced deviation of the C/N ratio estimated after exposure of Pd/WZ2 to the various gas mixtures at RT (Exps. 14 and 15). In this particular case, the underestimation of ΔCO_2 is most limited and the quantity of N_2O formed in the 250–500 °C is estimated to be 0.02 μmol m^{-2}, which leads to a C/N corrected ratio of 2.8.

4.3. Nature of the nitrogen-containing organic species

The exact nature of the organic nitrogen-containing species formed on the surface of the catalysts cannot be ascertained on the sole basis of the present results. Nevertheless valuable conclusions may be deduced from them.

The interaction of C_3H_6 with reducible W^{6+} centers, via a single electron transfer [25], most likely produces allylic radical species [33], the formation of which is greatly favored because of being resonantly stabilized:

$$CH_2{=}CH{-}CH_3 + W^{6+}{=}O^{2-} \rightarrow CH_2{=}CH{-}CH_2^{\bullet} + W^{5+}{-}OH^{-}. \quad (1)$$

The comparison of the C_3H_6 profiles from the TPSR and the TPO in C_3H_6–O_2–He indicates that this allylic radical species reacts readily with NO_x species, as indicated by the C_3H_6 deficit up to 60 °C in the TPSR in C_3H_6–O_2–He (Fig. 7). Although it is still uncertain whether these allylic radical species react with desorbing NO_2 [39] or with adsorbed nitrates [33,55], such interactions lead to the formation of adsorbed R–NO_x species such as nitropropene, the stoichiometry of which is consistent with the C/N ratio of 3 estimated previously:

$$CH_2{=}CH{-}CH_2^{\bullet} + {}^{\bullet}NO_2 \rightarrow CH_2{=}CH{-}CH_2{-}NO_2. \quad (2)$$

It has been reported in many studies that R–NO_x species transform to isocyanates [37,40,47,48,58,67–69], which would be key intermediates of HC-SCR. On WO_x–ZrO_2 based catalysts, however, the formation of isocyanates from R–NO_x compounds could not be detected when CH_4 was used as a reductant [39] and occurred to a very limited extent with C_3H_6 [33]. In addition, it has been suggested that isocyanates are highly reactive with respect to O_2 and NO + O_2 [33,47,48,50,58], leading ultimately to the formation of N_2 and N_2O. In the TPSR in C_3H_6–O_2–He (Figs. 3 and 4), the production of NO at temperatures greater than 250 °C may thus be attributed to the decomposition of R–NO_x species rather than isocyanate species, as the TPSR were carried out in the presence of a

large excess of O_2 and that a residual quantity of NO was detected in the gas phase.

Very few works reported that these R–NO_x species are stable up to temperatures well-above 250 °C. On Ag–Al_2O_3 and ZrO_2 samples, Meunier et al. and Matyshak et al. reported that adsorbed organic nitrogen-containing species are stable at temperatures at least as high as 400 °C under a complete C_3H_6–NO–O_2 mixture [53,56]. Hayes et al. showed that R–NO_x species formed on Cu-ZSM-5 by pulsing C_3H_6–NO–O_2 are stable at 300 °C as long as successive doses are provided, whereas they decompose at the latter temperature under an inert atmosphere [46]. In other studies, the rather low thermal stability of R–NO_x species may therefore be attributed to the experimental conditions under which these experiments were carried out. In most studies, the thermal stability of these species was investigated under vacuum [39,42,44,50,69,70] or inert atmospheres [41,53,71], both of which may promote the dehydration of R–NO_x to isocyanates [72]. In the temperature range in which R–NO_x decompose in the TPSR in C_3H_6–O_2–He, i.e. above 250 °C, full oxidation of C_3H_6 is observed on Pd/WZ which means that about 0.15% of water is also present in the feed. The experiments performed in the present work were carried out under conditions more representative of the HC-SCR reaction and may thus provide more accurate information on the thermal stability of the formed R–NO_x species. Additionally, it must be stressed that the thermal stability of R–NO_x formed via the reaction between NO_x and C_3H_6 may be rather difficult to assess accurately by FTIR. In particular, on acidic materials, the R–NO_x IR signature lies in the coke deposit region [33,55].

The NO_x profiles obtained in C_3H_6–O_2–He suggest the existence of two different R–NO_x species, as distinct NO_x peaks are observed at 320 and 520 °C on WZ and 300 and 440 °C on Pd/WZ1 (Fig. 3). Apart from the fact that the NO_x profiles are shifted to lower temperatures on Pd/WZ1, this phenomenon being more pronounced for the high-temperature peak, Pd promotion of WZ also induces significant differences in the distribution of the produced NO_x (NO or NO_2) species. Based on these differences, we assigned the low-temperature (LT) peak to the decomposition of C_3H_5–O–NO (propenyl nitrite), and the high-temperature (HT) peak to the decomposition of C_3H_5–NO_2 (nitropropene). Both of these compounds satisfy a C/N ratio of 3, as estimated previously. On the basis of FTIR, other studies also concluded to the dual formation of organo–nitrite and organo–nitrate species in the interaction between NO_x and propene [44,47,48,52–55]. The assignment of the LT peak to the decomposition of an organo–nitrite species, i.e. C_3H_5–O–NO, is in good agreement with previous studies of Zuzaniuk et al. [71]. These authors showed that the decomposition of *tert*-butyl nitrite produces NO_2 by cleavage of the C–O bond on Al_2O_3, whereas on Co- or Ag-promoted Al_2O_3, NO is mainly formed via O–N bond cleavage. It is suggested that the decomposition of the organo–nitro compound, i.e. C_3H_5–NO_2, occurs at greater temperatures because of its propensity to isomerize to its aci-form [39,45,72], which results in a more stable π-conjugated diene compound (Fig. 11). The decomposition of nitropropene should result in the release of NO_2, as for this species the C–N bond cleavage is the most likely. On WZ (Fig. 3a), however, the formation of large amounts of NO is also observed. At such elevated temperatures, this may be attributed to (i) thermodynamics related to the $NO_2 \rightleftharpoons NO + \frac{1}{2}O_2$ equilibrium and/or (ii) gas-phase interaction of NO_2 with C_3H_6 [36]. The fact that NO is exclusively observed at about 440 °C on Pd/WZ1 (Fig. 3b) may be accounted for the isomerization of the organo–nitro compound to organo–nitrite [69] and the decomposition of the latter leading to the release of NO mainly [71]. It is worthwhile to note that such a pathway has been recently suggested in the decomposition of CH_3–NO_2 on the basis of the NO detection by FTIR on Pd/WZ [39]. In contrast, the formation of NO could not be measured on the bare WZ support in the same study.

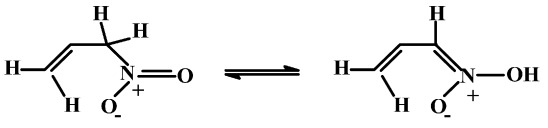

Fig. 11. Schematic representation of nitropropene in equilibrium with its aci-form.

In agreement with the latter work, or that of Haneda et al. on Al_2O_3-based catalysts [48], the results show that the decomposition of R–NO_x is promoted by the addition of a transition metal to WZ, here Pd. This promoting effect is, however, attributed to the isomerization of nitropropene to propenyl nitrite rather than the transformation of R–NO_x to isocyanates [48]. The decomposition of propenyl nitrite may be written as follows:

$$CH_2{=}CH{-}CH_2{-}O{-}NO \rightarrow CH_2{=}CH{-}CH_2O^{\bullet} + {}^{\bullet}NO. \quad (3)$$

The rearrangement of the $C_3H_5O^{\bullet}$ radical via a C–H β scission yields to the formation of acrolein and a $H^{\bullet}$ radical [Eq. (4)], which may recombine [Eq. (5)] with the proton created by $H^{\bullet}$ abstraction from C_3H_6 and W^{6+} oxidation [Eq. (1)], thus closing the catalytic sequence and leading to the overall Eq. (6).

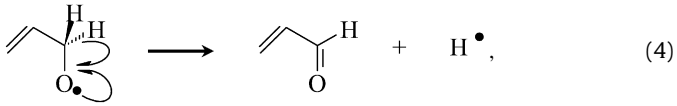

(4)

$$W^{5+}{-}OH^{-} + H^{\bullet} \rightarrow H_2 + W^{6+}{=}O^{2-}, \quad (5)$$

$$C_3H_6 + NO_2 \rightarrow C_3H_4O + H_2 + NO. \quad (6)$$

This latter equation stresses the formation of partially oxidized hydrocarbons by the reaction between NO_2 and C_3H_6. NO_2–HC gas-phase experiments also showed the formation of acrolein when C_3H_6 is used [36] or that of various mildly oxidized hydrocarbons when light alkanes react with NO_2 [73,74]. Recently, it was proposed that the interaction of CH_4 and NO_2 yields formaldehyde on Pd/WO_x–ZrO_2 [39].

4.4. R–NO_x as active intermediates or spectators of C_3H_6-SCR on Pd/WZ catalysts?

C_3H_6-SCR activity is likely attributable to Pd^0 sites on which NO dissociation occurs, followed by cleaning of oxygen from the metal surface by C_3H_6 oxidation [35,75,76]. This contradicts previous characterization of the Pd species deposited on tungstated zirconia supports reported by Chin et al. [28,29]. From DRIFTS studies of NO, these authors reported that WZ stabilizes Pd^{2+} isolated ions. It must be stressed, however, that these DRIFTS results were obtained after activation of the samples at elevated temperatures under He. This activation procedure differs markedly from the experimental conditions under which C_3H_6-SCR is carried out, that is the absence of propene in the reaction mixture. It is known that even in excess O_2, oxidized Pd species may be reduced to Pd^0 clusters in the presence of C_3H_6 depending on the nature of the supporting oxide [60,77]. In the present study, the reduction of oxidized Pd species under C_3H_6-containing mixtures is supported by (i) the elevated selectivity in N_2O, close to 50%, which agrees well with that found on Pd^0/SiO_2 [78], (ii) the fact that NO inhibits C_3H_6 oxidation by about 40–50 °C (Fig. 7), which is in accord with previous work of Burch and Millington [78], and (iii) the rather different steady-state conversions obtained at temperatures below 230 °C (Fig. 10, Section 3.2.5). These experiments also indicate that oxidized Pd species are reduced at temperatures between 210 and 230 °C under the complete NO–O_2–C_3H_6–He feed. Thus,

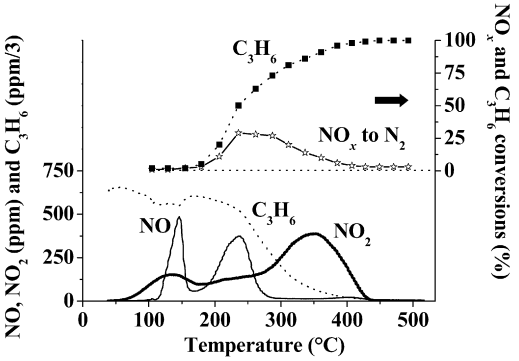

Fig. 12. Steady-state catalytic conversions of C_3H_6 (■) and NO_x to N_2 (☆) in the course of the C_3H_6–NO–O_2–N_2 reaction (1900 ppm—340 ppm—8%—balance), NO_2 profile for the TPD in N_2 and NO profile for the TPSR in C_3H_6–O_2–N_2 (1900 ppm—8%—balance) on $Pd/Ce_{0.68}Zr_{0.32}O_2$ (data from Ref. [60]).

this work provides confirmation of the zero-valent oxidation state of Pd under C_3H_6-SCR operating conditions, such an assumption having been evoked previously by Chin et al. [29]. On Pt^0/SiO_2 catalysts, Burch and co-workers [79,80] provided further insights in the NO dissociation mechanism of the NO–C_3H_6–O_2 reaction through SSITKA-MS (steady-state isotopic transient kinetic analysis coupled with mass spectrometry). In this mechanism, N_{ads} species is considered as an active species leading to N_2. In this reaction, however, the SSITKA-MS technique could not provide additional information on the detailed formation of N_2 because of the lifetimes of the reaction intermediates being too short under these particular experimental conditions [80].

Consequently, this suggests that the R–NO_x compounds formed under the present experimental conditions are not active intermediates in the C_3H_6-SCR reaction on Pd/WZ catalysts but are more likely spectators. The fact that the temperatures at which these species decompose on Pd/WZ (Fig. 3b, $T > 270\,^{\circ}C$) do not coincide with that at which deNO_x starts (Fig. 10, $T > 190\,^{\circ}C$) would be in agreement with such a conclusion. One must however be extremely careful when trying to correlate results obtained under different experimental conditions, which is typically the case when comparing TPSR and steady-state data. SSITKA-MS and SSITKA-DRIFT (steady-state isotopic transient kinetic analysis coupled with diffuse reflectance FT-IR) would obviously be of the greatest interest to ascertain the spectator character of the R–NO_x compounds formed on Pd/WZ.

4.5. Correlation between TPSR of preadsorbed NO_x in C_3H_6–O_2 and C_3H_6-SCR on non-zero-valent Pd species

Next, we consider the above findings about the formation–decomposition of R–NO_x in C_3H_6-SCR on Pd/WZ catalysts together with results reported previously for Pd catalysts supported on $Ce_{0.68}Zr_{0.32}O_2$ [60]. On the latter catalysts, it was concluded that oxidized Pd species do not reduce to Pd^0 clusters due to interaction with the ceria–zirconia support, and that R–NO_x species are involved in the C_3H_6-SCR reaction by providing mildly oxidized hydrocarbons as the "effective" reducers of NO_x. In the proposed C_3H_6-SCR mechanism [60], it must be stressed that the formed R–NO_x species do not react with NO_x to yield N_2, only their decomposition is important. In this particular context an attempt of comparison of the TPSR of preadsorbed NO_x in C_3H_6–O_2–He and C_3H_6-SCR can be made, since the presence of NO_x is no longer required in the gas phase during the TPSR to get the SCR going through the coupling of N-containing molecules as proposed by Smits and Iwasawa [81].

Fig. 12 shows the steady-state conversion of NO_x to N_2 and conversion of C_3H_6 (top), together with the TPD and TPSR profiles obtained in N_2 and C_3H_6–O_2–N_2 (1900 ppm—8%—balance), respectively, after exposure of $Pd(0.89)/Ce_{0.68}Zr_{0.32}O_2$ to NO–O_2–N_2 (340 ppm—8%—balance) at RT (bottom). For the sake of clarity, only the major released NO_x species are shown in Fig. 12, i.e. NO_2 and NO for the TPD in N_2 and TPSR in C_3H_6–O_2–N_2, respectively (for more details please refer to [60]). As is the case for the TPSR experiments carried out on Pd/WZ, a drastic modification of the NO_x profiles is observed on $Pd(0.89)/Ce_{0.68}Zr_{0.32}O_2$ (bottom of Fig. 12). In an inert atmosphere, such as N_2, NO_2 is the major desorbed product, whereas NO is the major species produced in the TPSR in C_3H_6–O_2–N_2. In contrast to what is observed for Pd/WZ catalysts, however, NO is formed at lower temperatures than NO_2 on $Pd(0.89)/Ce_{0.68}Zr_{0.32}O_2$. The two NO peaks have been attributed to the decomposition of R–NO_x species, as in this low temperature domain NO_2 hardly interacts with C_3H_6 in the gas phase [36]. It is worthwhile to note that the profile of the second NO peak parallels the steady-state C_3H_6-SCR activity (top of Fig. 12) from 170 to 245 °C and that this latter temperature corresponds both to the maxima of the NO peak and steady-state deNO_x activity. This rather good correlation provides additional support to the mechanism proposed previously on $Pd/Ce_{0.68}Zr_{0.32}O_2$ catalysts [60].

5. Conclusion

The main points which come from this study are as follows:

- On WO_x–ZrO_2 based catalysts, the fact that NO_x profiles are observed at much greater temperatures in the TPSR in C_3H_6–O_2–He than in the TPSR in O_2–He testifies unambiguously of the decomposition of organic nitrogen-containing species formed through the interaction of C_3H_6 and ad-NO_x.
- From the temperature-programmed transient experiments, the C/N ratio of these organic nitrogen-containing species was estimated to be 3.
- In the TPSR in C_3H_6–O_2–He, we propose that the low-temperature NO peak is assigned to the decomposition of propenyl nitrite (C_3H_5–O–NO), whereas the high-temperature peak is due to the decomposition of nitropropene (C_3H_5–NO_2), both of which satisfy a C/N ratio of 3, as estimated previously. The addition of Pd to WO_x–ZrO_2 promotes the decomposition of nitropropene, with a significant lowering of the decomposition temperature, whereas that of propenyl nitrite is hardly affected. Based on the differences in NO_x distributions between WO_x–ZrO_2 and Pd/WO_x–ZrO_2, the promoting effect of Pd was inferred to be the isomerization of nitropropene to propenyl nitrite.
- This work provides confirmation of the zero-valent oxidation state of Pd on Pd/WO_x–ZrO_2 under C_3H_6-SCR operating conditions. The observed activity in C_3H_6-SCR is ascribed to Pd^0 sites according to the well-established decomposition mechanism of NO on zero-valent platinum group metals [35,75,76,79,80]. Consequently, this suggests that the R–NO_x compounds formed under the present experimental conditions are not active intermediates in the C_3H_6-SCR reaction on Pd/WZ catalysts but are more likely spectators. The fact that the temperatures at which these species decompose on Pd/WZ do not coincide with that at which deNO_x starts would be in agreement with such a conclusion. One must however be extremely careful when trying to correlate results obtained under different experimental conditions, which is typically the case when comparing TPSR and steady-state data. SSITKA-MS and SSITKA-DRIFT would obviously be of the greatest interest to ascertain the spectator character of the R–NO_x compounds formed on Pd/WZ.

Particular emphasis is also put on critical discussion of previous studies reported in the literature where characterization of the catalysts have been carried out under experimental conditions rather different from those representative of C_3H_6-SCR, which may lead to debatable conclusions.

In light of these findings about the formation–decomposition of R–NO_x, results reported previously for Pd catalysts supported on $Ce_{0.68}Zr_{0.32}O_2$ [60] are widened. On these catalysts, Pd oxidized species do not reduce due to the interaction with the support and R–NO_x were proposed to be intermediates of C_3H_6-SCR. A rather good correlation between NO production in the TPSR in C_3H_6–O_2 and steady-state C_3H_6-SCR activity is observed, which provides further support to the mechanism proposed previously on Pd/$Ce_{0.68}Zr_{0.32}O_2$ catalysts [60].

Acknowledgments

Dr. X. Carrier is acknowledged for his recommendations regarding the synthesis of the catalyst samples. The authors thank Dr. H.Y. Law for critical reading of the manuscript. Also, we would like to thank MEL Chemicals for kindly providing the zirconium oxyhydroxide starting material (XZO880/01).

References

[1] M. Hino, K. Arata, Chem. Commun. (1988) 1259.
[2] R.A. Boyse, E.I. Ko, J. Catal. 171 (1997) 191, and references therein.
[3] M. Scheithauer, R.K. Grasselli, H. Knözinger, Langmuir 14 (1998) 3019.
[4] D.G. Barton, S.L. Soled, G.D. Meitzner, G.A. Fuentes, E. Iglesia, J. Catal. 181 (1999) 57.
[5] D.G. Barton, M. Shtein, R.D. Wilson, S.L. Soled, E. Iglesia, J. Phys. Chem. B 103 (1999) 630.
[6] J.C. Vartuli, J.G. Santiesteban, P. Traverso, N. Cardona-Martinez, C.D. Chang, S.A. Stevenson, J. Catal. 187 (1999) 131.
[7] N. Naito, N. Katada, M. Niwa, J. Phys. Chem. B 103 (1999) 7206.
[8] C.D. Baertsch, S.L. Soled, E. Iglesia, J. Phys. Chem. B 105 (2001) 1320.
[9] K. Shimizu, T.N. Venkatraman, W. Song, Appl. Catal. A Gen. 224 (2002) 77.
[10] S. Kuba, M. Che, R.K. Grasselli, H. Knözinger, J. Phys. Chem. B 107 (2003) 3459.
[11] T.N. Vu, J. van Gestel, J.P. Gilson, C. Collet, J.P. Dath, J.C. Duchet, J. Catal. 231 (2005) 453.
[12] T. Onfroy, G. Clet, M. Houalla, J. Phys. Chem. B 109 (2005) 3345.
[13] L.M. Petkovic, J.R. Bielenberg, G. Larsen, J. Catal. 178 (1998) 533.
[14] M. Scheithauer, T.-K. Cheung, R.E. Jentoft, R.K. Grasselli, B.C. Gates, H. Knözinger, J. Catal. 180 (1998) 1.
[15] S.D. Rossi, G. Ferraris, M. Valigi, D. Gazzoli, Appl. Catal. A Gen. 231 (2002) 173.
[16] S. Kuba, P. Lukinskas, R. Ahmad, F.C. Jentoft, R.K. Grasselli, B.C. Gates, H. Knözinger, J. Catal. 219 (2003) 376.
[17] G. Larsen, E. Lotero, S. Raghavan, R.D. Parra, C.A. Querini, Appl. Catal. A Gen. 139 (1996) 201.
[18] S.R. Vaudagna, R.A. Comelli, N.S. Figoli, Appl. Catal. A Gen. 164 (1997) 265.
[19] D.G. Barton, S.L. Soled, E. Iglesia, Top. Catal. 6 (1998) 87.
[20] G. Fitzsimons, J.K.A. Clarke, M.R. Smith, J.J. Rooney, Catal. Lett. 52 (1998) 69.
[21] S. Kuba, B.C. Gates, R.K. Grasselli, H. Knözinger, Chem. Commun. (2001) 321.
[22] P. Lukinskas, S. Kuba, B. Spliethoff, R.K. Grasseli, H. Knözinger, Top. Catal. 23 (2003) 163.
[23] X. Carrier, P. Lukinskas, S. Kuba, L. Stievano, F.E. Wagner, M. Che, H. Knözinger, Chem. Phys. Chem. 5 (2004) 1191.
[24] T.N. Vu, J. van Gestel, J.P. Gilson, C. Collet, J.P. Dath, J.C. Duchet, J. Catal. 231 (2005) 468.
[25] S. Kuba, P.C. Heydorn, R.K. Grasselli, B.C. Gates, M. Che, H. Knözinger, Phys. Chem. Chem. Phys. 3 (2001) 146.
[26] E. Iglesia, D.G. Barton, S.L. Soled, S. Miseo, J.E. Baumgartner, W.E. Gates, G.A. Fuentes, G.D. Meitzner, Stud. Surf. Sci. Catal. 101 (1996) 533.
[27] R.D. Wilson, D.G. Barton, C.D. Baertsch, E. Iglesia, J. Catal. 194 (2000) 175.
[28] Y.-H. Chin, W.A. Alvarez, D.E. Resasco, Catal. Today 62 (2000) 159.
[29] Y.-H. Chin, W.A. Alvarez, D.E. Resasco, Catal. Today 62 (2000) 291.
[30] K. Okumara, T. Kusakabe, M. Niwa, Chem. Lett. 10 (2001) 1018.
[31] K. Okumara, T. Kusakabe, M. Niwa, Appl. Catal. B Environ. 41 (2003) 137.
[32] D. Yang, J. Li, M. Wen, C. Song, Catal. Commun. 8 (2007) 2243.
[33] T. Weingand, S. Kuba, K. Hadjiivanov, H. Knözinger, J. Catal. 209 (2002) 539.
[34] V.I. Pârvulescu, P. Grange, B. Delmon, Catal. Today 46 (1998) 233.
[35] R. Burch, J.P. Breen, F.C. Meunier, Appl. Catal. B Environ. 39 (2002) 283.
[36] O. Gorce, F. Baudin, C. Thomas, P. Da Costa, G. Djéga-Mariadassou, Appl. Catal. B Environ. 54 (2004) 69.
[37] B. Djonev, B. Tsyntsarski, D. Klissurski, K. Hadjivanov, J. Chem. Soc. Faraday Trans. 93 (1997) 4055.
[38] T. Sun, M.D. Fokema, J.Y. Ying, Catal. Today 33 (1997) 251.
[39] M. Kantcheva, I. Cayirtepe, Catal. Lett. 115 (2007) 148.
[40] Y.H. Yeom, M. Li, W.M.H. Sachtler, E. Weitz, J. Catal. 238 (2006) 100.
[41] T. Chafik, S. Kameoka, Y. Ukisu, T. Miyadera, J. Mol. Catal. A Chem. 136 (1998) 203.
[42] Y. Ukisu, S. Sato, G. Muramatsu, K. Yoshida, Catal. Lett. 11 (1991) 177.
[43] H. Yasuda, T. Miyamoto, C. Yokoyama, M. Misono, Shokubai 35 (1993) 398.
[44] T. Tanaka, T. Okuhara, M. Misono, Appl. Catal. B 4 (1994) L1.
[45] G. Centi, A. Galli, S. Perathoner, J. Chem. Soc. Faraday Trans. 92 (1996) 5129.
[46] N.W. Hayes, R.W. Joyner, E.S. Shpiro, Appl. Catal. B 8 (1996) 343.
[47] T. Okuhara, Y. Hasada, M. Misono, Catal. Today 35 (1997) 83.
[48] M. Haneda, Y. Kintaichi, M. Inaba, H. Hamada, Catal. Today 42 (1998) 127.
[49] A. Satsuma, T. Enjoji, K.-I. Shimizu, K. Sato, H. Yoshida, T. Hattori, J. Chem. Soc. Faraday Trans. 94 (1998) 301.
[50] S. Sumiya, H. He, A. Abe, N. Takezawa, K. Yoshida, J. Chem. Soc. Faraday Trans. 94 (1998) 2217.
[51] F.C. Meunier, V. Zuzaniuk, J.P. Breen, M. Olsson, J.R.H. Ross, Catal. Today 59 (2000) 287.
[52] Y. Chi, S.S.C. Chuang, J. Catal. 190 (2000) 75.
[53] F.C. Meunier, J.P. Breen, V. Zuzaniuk, M. Olsson, J.R.H. Ross, J. Catal. 187 (1999) 493.
[54] B.I. Mosqueda-Jiménez, A. Jentys, K. Seshan, J.A. Lercher, Appl. Catal. B Environ. 46 (2003) 189.
[55] C. Sedlmair, B. Gil, K. Seshan, A. Jentys, J.A. Lercher, Phys. Chem. Chem. Phys. 5 (2003) 1897.
[56] V.A. Matyshak, V.F. Tre'yakov, K.A. Chernyshev, T.N. Burdeinaya, V.N. Korchak, V.A. Sadykov, Kinet. Catal. 47 (2006) 593.
[57] H.-Y. Chen, T. Voskoboinikov, W.M.H. Sachtler, Catal. Today 54 (1999) 483.
[58] K. Hadjiivanov, H. Knözinger, B. Tsyntsarski, L. Dimitrov, Catal. Lett. 62 (1999) 35.
[59] R. Brosius, P. Bazin, F. Thibault-Starzyk, J.A. Martens, J. Catal. 234 (2005) 191.
[60] C. Thomas, O. Gorce, C. Fontaine, J.-M. Krafft, F. Villain, G. Djéga-Mariadassou, Appl. Catal. B Environ. 63 (2006) 201.
[61] F.R. Chen, G. Coudurier, J.F. Joly, J.C. Védrine, J. Catal. 143 (1993) 616.
[62] W. Stichert, F. Schüth, Chem. Mater. 10 (1998) 2020.
[63] E.V. Rebrov, A.V. Simakov, N.N. Sazanova, V.A. Rogov, G.B. Barannik, Catal. Lett. 51 (1998) 27.
[64] R. Burch, E. Halpin, J.A. Sullivan, Appl. Catal. B 17 (1998) 115.
[65] F. Baudin, P. Da Costa, C. Thomas, S. Calvo, Y. Lendresse, S. Schneider, G. Djéga-Mariadassou, Top. Catal. 30–31 (2004) 97.
[66] N.W. Hayes, W. Grünert, G.J. Hutchings, R.W. Joyner, E.S. Shpiro, J. Chem. Soc. Chem. Commun. (1994) 531.
[67] Y. Ukisu, S. Sato, A. Abe, K. Yoshida, Appl. Catal. B 2 (1993) 147.
[68] M. Iwamoto, H. Takeda, Catal. Today 27 (1996) 71.
[69] S. Kameoka, T. Chafik, Y. Ukisu, T. Miyadera, Catal. Lett. 51 (1998) 11.
[70] M. Yamaguchi, J. Chem. Soc. Faraday Trans. 93 (1997) 3581.
[71] V. Zuzaniuk, F.C. Meunier, J.R.H. Ross, J. Catal. 202 (2001) 340.
[72] A.D. Cowan, N.W. Cant, B.S. Haynes, P.F. Nelson, J. Catal. 176 (1998) 329.
[73] K. Otsuka, R. Takahashi, K. Amakawa, I. Yamanaka, Catal. Today 45 (1998) 23.
[74] K. Otsuka, R. Takahashi, I. Yamanaka, J. Catal. 185 (1999) 182.
[75] R. Burch, P.J. Millington, A.P. Walker, Appl. Catal. B Environ. 4 (1994) 65.
[76] R. Burch, T.C. Watling, Catal. Lett. 43 (1997) 19.
[77] M. Fernàndez-Garcia, A. Iglesia-Juez, A. Martínez-Arias, A.B. Hungría, J.A. Anderson, J.C. Conesa, J. Soria, J. Catal. 221 (2004) 594.
[78] R. Burch, P.J. Millington, Catal. Today 29 (1996) 37.
[79] R. Burch, A.A. Shestov, J.A. Sullivan, J. Catal. 182 (1999) 497.
[80] R. Burch, Top. Catal. 24 (2003) 97.
[81] R.H.H. Smits, Y. Iwasawa, Appl. Catal. B Environ. 6 (1995) L201.